

5 Quantum Well States beyond the single particle model

For many aspects of the interpretation of data from quantum well states, the electrons can be regarded as non-interacting. In the previous chapters, this picture has proven sufficient. However, with increasing spectral resolution, effects become evident which suggest the influence of interaction between quasiparticles; here two such effects will be presented. In Pb films formed on Si(111), electron localization is observed in the direction parallel to the surface. Under certain circumstances, this localization may lead to electron correlation in the quantum well. For In/Si(111), coupling between electrons and phonons is observed, using the high angular and energy resolution provided by the new generation of imaging type electron energy analyzers.

Both the abovementioned effects can be measured with angle resolved photoemission spectroscopy, but cannot be incorporated into the simplified three-step model of photoemission described in Chapter 2. In this model each electron is treated as an independent particle in a continuous background of other electrons. In reality the remaining electrons will respond to the formation of the core hole. Furthermore, the interaction between electrons and other excitations is ignored, whereas electron-electron and electron-phonon interaction should be included. In order to explain the influence of these effects on photoemission data, I will here give a more formal description of the photoemission process¹.

The transition probability w for an optical transition between the ground state Ψ_i and one of the possible final states Ψ_f can be approximated by Fermi's golden rule:

$$w = \frac{2\pi}{\hbar} \left| \langle \Psi_f | H_{\text{int}} | \Psi_i \rangle \right|^2 \delta(E_f - E_i - h\nu). \quad (5.1)$$

In this equation E_f and E_i are the final- and initial state energies, respectively. The interaction with the photon is treated as a perturbation that can be represented by

$$H_{\text{int}} = -\frac{e}{mc} \mathbf{A} \cdot \mathbf{p}, \quad (5.2)$$

where \mathbf{A} is the electromagnetic vector potential and \mathbf{p} is the electron momentum operator. These quantities depend on the geometry of the experiment, the polarization of the photon and the details

¹ See for example: A. Damascelli, Z. Hussain, and Z.X. Shen, Rev. of Mod. Phys. **75**, 473 (2003); S. Hüfner, Photoelectron Spectroscopy, 2nd ed. Berlin; Springer, 1996; S. D. Kevan, ed., Angle-Resolved Photoemission: Theory and Current Applications, Amsterdam; Elsevier 1992; G. D. Mahan, and E.W. Plummer Many-body Effects in Photoemission, pg 953-987, (2000) Handbook of Surface Science, Vol. 2, Edited by Horn and Scheffler (Elsevier Science Pub.).

of the wave functions. The initial and final state wave functions can be expressed as the product of the one-electron state Φ_{if} and the state of the $N - 1$ remaining electrons

$$\Psi_{i/f}(N) = \Phi_{i/f\mathbf{k}} \Psi_{i/f\mathbf{k}}(N-1). \quad (5.3)$$

In this context it is relevant that $\Psi_i(N-1)$ is not an eigenstate of the $N-1$ system, but a state of the original system when one electron has been removed. The total photoemission intensity in an experiment can be obtained by summing all the transition probabilities for all the initial and final states. Combining this concept with Equation 5.1 and 5.3 the total intensity $I(\mathbf{k}, E)$ becomes:

$$I(\mathbf{k}, E) \propto \sum_{f,i} \left| \langle \Phi_f | H_{\text{int}} | \Phi_i \rangle \right|^2 A(\mathbf{k}, E), \quad (5.4)$$

where $A(\mathbf{k}, E)$ is the spectral function. This is actually the spectrum that is measured in photoemission, and can be represented as

$$A(\mathbf{k}, E) = \sum_s |c_s|^2 \delta(E_F + E_s(N-1) - E_0(N) - \hbar\nu). \quad (5.5)$$

In this equation, $|c_s|^2 = \left| \langle \Psi_s(N-1) | \Psi_i(N-1) \rangle \right|^2$ is the probability that when an electron is removed, the system with $(N-1)$ electrons will remain in the excited state s . For a non-interacting system, this probability will be unity for one excited state s_0 , and zero for all others. Assuming an allowed transition, the ARPES spectrum consists of a sharp peak in this case. For correlated systems, $|c_s|^2$ will be non-zero for many of the possible final states, because the removal of an electron changes the effective potential and leads to an overlap of many of the new initial states of the $(N-1)$ electron system and the possible eigenstates. In this case the ARPES spectrum may show additional features, depending on the number of excited states.

In order to simplify the treatment, the actual wavefunction is replaced by the Green function $G(\mathbf{k}, E)$. Corrections to the Green function that originate from interaction effects can be represented by the electron self-energy $\Sigma(\mathbf{k}, E) = \text{Re}\Sigma(\mathbf{k}, E) + \text{Im}\Sigma(\mathbf{k}, E)$. The real part of the self-energy represents how the energies are changed, and the imaginary part how the lifetime of an electron propagating through an interacting system changes. For a non-interacting system, the self-energy will be equal to zero. When the Green function and the spectral function are expressed in terms of the self-energy, the first indicates how the binding energies are modified, and the latter indicates what the spectral lines will look like. This results in the following set of equations:

$$G(\mathbf{k}, E) = \frac{1}{E - E_{\mathbf{k}} - \Sigma(\mathbf{k}, E)} \quad (5.6)$$

and

$$A(\mathbf{k}, E) = \frac{1}{\pi} \frac{\text{Im}\Sigma(\mathbf{k}, E)}{[E - E_{\mathbf{k}} - \text{Re}\Sigma(\mathbf{k}, E)]^2 + [\text{Im}\Sigma(\mathbf{k}, E)]^2}, \quad (5.7)$$

where $E_{\mathbf{k}}$ is the energy of an electron with wave vector \mathbf{k} , thus representing the band structure of the studied material. From a comparison of the two equations given above, it can be concluded that $A(\mathbf{k}, E) = 1/\pi \text{Im}G(\mathbf{k}, E)$. This means that, in principle, the self-energy can be extracted from the photoemission data, and that ARPES data can be simulated when the self-energy is known.

There are several contributions to the self-energy, for example interactions between electrons and electrons, electrons and phonons, electrons and impurities, and electrons and magnons. The terms in the self-energy corresponding to these interactions, can to the lowest order be summed up to obtain the total self-energy. Each of these contributions has its own different energy scale, which, in many cases, allows for a separation of the interaction effects. As has been shown in this work, ARPES can be used to measure the full band structure with high energy and angular resolution. From a careful study of the obtained electronic structure, and the deviations from a non-interacting system, interaction effects can be identified. The determination of such interaction effects with high resolution angle-resolved photoemission is an important trend in current photoemission work. One of the main driving forces is the search for a better understanding of superconductivity², and many other fundamental physical processes³.

2 T. Valla et al. Phys. Rev. Lett. **92**, 86401 (2004); H. Matsui et al. Phys. Rev. Lett. **94**, 47005 (2005); H.-B. Yang et al. Phys. Rev. Lett. **92**, 246403 (2004); N.P. Armitage et al. Phys. Rev. Lett. **88**, 257001 (2002).

3 R. Cortés et al. Phys. Rev. Lett. **96**, 126103 (2006); J.E. Gayone et al. Phys. Rev. Lett. **91**, 127601 (2003); D. Qian et al. Phys. Rev. Lett. **96**, 046407 (2006).

5.1 Electron localization and correlation effects in Pb/Si(111)

In extended metal films, electron motion is only confined in the (z-) direction normal to the film. Hence quantum well states are expected to exhibit a dispersion relation $E(k_{\parallel x}, k_{\parallel y})$ for the component of the electron wave vector k_{\parallel} along the x and y directions parallel to the film that is similar to the bulk band from which they are derived. This is in fact found in studies of quantum well states in s-p metals such as Ag⁴, Al⁵, and Mg⁶. In the present work this is shown from the results for Pb and Al on graphite (Figures 3.11 and 3.29) and for In on Si(100) and Si(111) (Figures 4.3 and 4.14). In this section I will discuss the only system that seems to be an exception to this behaviour: Pb on Si(111).

Figure 5.1 shows a comparison between data obtained for an as-deposited 15 ML thick layer of Pb on Si(111)7x7 (a), the same layer after annealing (b), Pb on Si(111) $\sqrt{3}$ (c), and an annealed layer of Pb on Cu(111) (d). All images are measured using the same photon energy of 24 eV, except for the image of Pb/Si(111)7x7 before annealing, where $h\nu = 26$ eV. The change in data quality between the as-deposited and annealed layer on Si(111)7x7 is consistent with the influence that annealing has on this system, as shown in Chapter 3. The broad feature at approximately 1 eV is the bulk-like feature due to incoherent scattering at the interface, as discussed in the previous chapter. The slightly higher photon energy is needed in order to separate this feature from the QWS around 0.5 eV; in order to compensate for the low contrast, this state is marked by a dashed line. For the annealed Pb layer on Si(111)7x7 and the Pb layer deposited on Si(111) $\sqrt{3}$ the region of hybridization with the substrate bands is easily distinguished from the part of the QWS that is not affected by the substrate bands. The relevance of this separation will be discussed in more

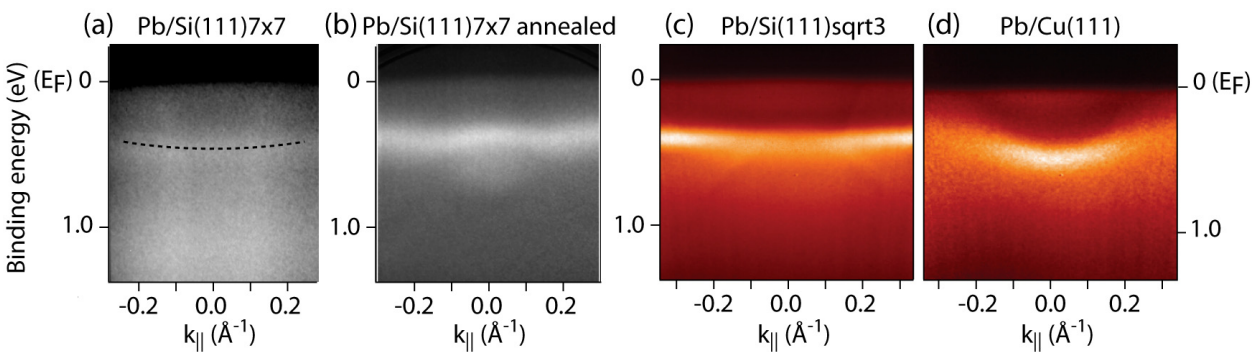


Figure 5.1: Photoemission images centred around normal emission for a 15 ML thick Pb film on (a) Si(111)7x7, (b) the same layer after annealing, (c) Pb on Si(111) $\sqrt{3}$, and (d) an annealed layer of Pb on Cu(111). Image (a) has been obtained at a photon energy of 26 eV, the other images at 24 eV.

4 M.A. Mueller, T. Miller, and T.-C. Chiang, Phys. Rev. B **41**, 5214 (1990).

5 L. Aballe, C. Rogero, S. Gokhale, S. Kulkarni and K. Horn, Surface Science, **482 - 485**, 488 (2001).

6 L. Aballe, C. Rogero, and K. Horn, Phys. Rev. B **65**, 125319 (2002).

detail below. It is important to note that the annealed Pb layer on Si(111)7x7 is not the same as a freshly deposited layer on Si(111) $\sqrt{3}$; the annealing temperature is far below the temperature needed to create the $\sqrt{3}\times\sqrt{3}$ reconstruction.

From a comparison of the images in Figure 5.1, it is clear that Pb/Cu(111) is different from the other systems. It shows a free electron like behaviour comparable to expectations from calculations and other systems. The features due to the QWS in the other images are almost flat and show only a small dispersion. In order to allow for a quantitative comparison of the dispersion of the QWS, effective masses m^* are used to describe the dispersion with the parallel component of the wave vector k_{\parallel} in these bands, $E = \hbar^2 k_{\parallel}^2 / 2m^*$. Hence, the value of the effective mass is inversely proportional to the curvature of the band; a higher effective mass indicates a flatter band. The values of the effective mass are usually expressed in units of the free electron mass m_e . From DFT calculations for freestanding Pb slabs, effective masses varying from 0.6 m_e at 4 eV below E_F to 2 m_e at 6 eV above E_F are expected. Depending on the exact coverage, m^* varies between 0.9 and 1.2 m_e in the energy region studied here. For the QWS in Pb/Cu(111) an effective mass of 1.2 m_e is derived, which corresponds very well to calculations. The effective mass of the other systems in Figure 5.1 is around 6 m_e ; an enormous deviation from expectations. That this high effective mass is not limited to a coverage of 15 ML can be confirmed by the images displayed in Figure 3.10; the curvature of the band only increases slightly towards higher coverages. This decrease of the effective mass is expected, because in the bulk limit of very thick films the effective mass should correspond to the in-plane effective mass of bulk Pb, which is approximately equal to m_e .

In order to analyze the dispersion of the quantum well state in more detail, and to exclude any artefacts due to a consideration of a limited range of k_{\parallel} , Figure 5.2 shows the photoemission intensity distribution for a 10 ML Pb film on Si(111) $\sqrt{3}$ along the $\bar{\Gamma} - \bar{M}$ direction in the 2-D Brillouin zone. Superimposed on this image is the calculated band dispersion for a 10 ML thick

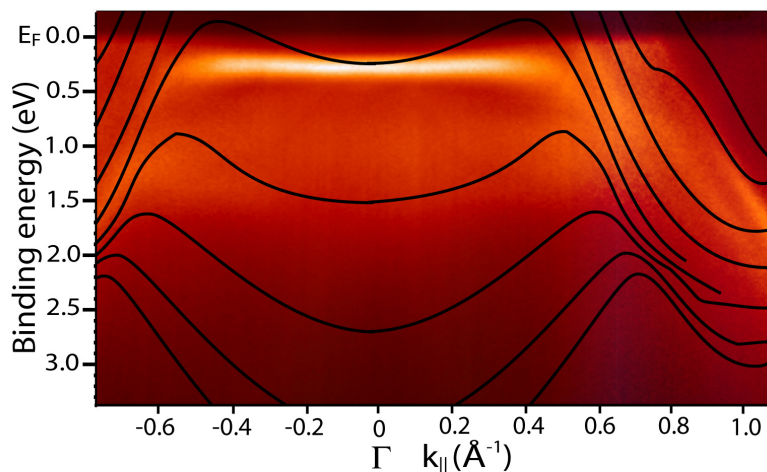
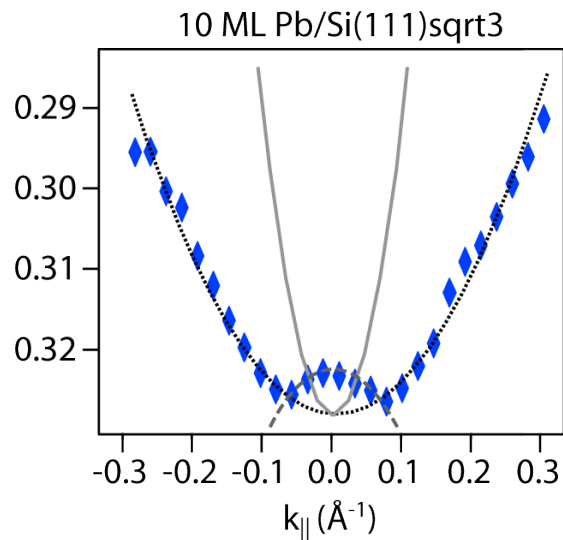


Figure 5.2: Cut through the surface Brillouin zone for a 10 ML thick Pb layer on Si(111) $\sqrt{3}$ obtained at a photon energy of 24 eV. Superimposed is the calculated band structure of a 10 ML thick free-standing Pb slab. Note the large discrepancy between the measured and calculated band dispersion around the zone centre.

free-standing Pb layer. The match between measurement and calculation is good for the downward dispersing $6p_{x,y}$ derived bands. The only discrepancy is the curvature of the QWS around the zone centre; the calculation shows a free-electron-like dispersion, while the measured QWS is almost flat. In Section 4.4 it was shown that hybridization between the substrate band and the QWS in the metal overlayer can substantially alter the shape of the QWS, to the point that in specific regions of the SBZ a downward dispersion can be observed. To perform an accurate measurement of the effective mass, the effects due to this hybridization have to be identified and separated from the rest of the QWS. Because of the high energy and angular resolution provided by the analyser, this discrimination is possible. To this end, cuts through the image along the energy direction have been taken every 0.023 \AA^{-1} , resulting in a set of regularly spaced EDCs. The binding energy position of the QWS as a function of k_{\parallel} were then obtained by fitting every individual spectrum. The result of this procedure for the 10 ML thick Pb film on $\text{Si}(111)\sqrt{3}$ is displayed in Figure 5.3. In order to observe fine details, the energy scale is strongly magnified compared to Figure 5.2.

Figure 5.3: Binding energy positions obtained by fitting the QWS in Figure 5.2 as described in the text (diamonds), with a fitted parabola to extract the effective mass (dotted line). The hybridization with the Si valance band maximum can be distinguished (dashed line). As a comparison, the free-electron-like parabola expected from calculations and the bulk band structure is shown (solid line).



The general shape of the QWS is an upward dispersing parabola, as would be expected for an s-p band derived state in a metal film. At the bottom of this parabola, a small downward dispersing feature can be distinguished, as indicated by the dashed line. This bump is due to the hybridization to the Si substrate band, having the shape of the topmost Si valence band, and has to be taken into account to determine the effective mass. Notice that in the raw data this feature is too small to be clearly visible. For the parabolic fit of the Pb-derived band to extract the curvature, indicated by the upward dispersing dotted line, these data points are ignored. This yields an effective mass of $8 m_e$ for the Pb band, more than 6 times as large as expected from calculations and from our observations in the Pb/Cu(111) system. When hybridization with the substrate bands is not taken into account, the obtained effective mass would seem to be even larger, but this would of course be incorrect. In order to stress the difference in curvature between the measured QWS and predictions from theory, the free electron parabola has been added to Figure 5.3 (solid parabola). These results

show that it is not only *possible* to discriminate between features induced by the substrate and the unaltered QWS, but it is *mandatory* in order to obtain a reliable value for the effective mass. For all the effective masses presented in this work, this effect has been taken into account.

Figure 5.4 shows the measured in-plane effective mass for Pb on Si(111) $\sqrt{3}$ (circles and triangles), In on Si(111) (squares), and from theory for free-standing Pb slabs (diamonds), as a function of binding energy (a) and film thickness (b). For the determination of the QWS binding energy, the bottom of the fitted parabola is used, rather than the peak position at the zone centre. The difference between the effective mass measured for Pb and In layers is very large; the values obtained for In closely resemble the theoretical expectations. As a function of coverage, the trend in the Pb effective mass is governed by a decrease towards the bulk limit. However, even for a film of 22 ML of Pb on Si(111) $\sqrt{3}$ the effective mass of the highest occupied QWS is still $5.2 m_e$, about five times as large as predictions from theory. From Figure 5.1 it is clear that this high effective mass is *not* a result of the interface reconstruction, because the same effect is observed for the as-deposited and annealed Pb layers on bare Si(111) 7×7 .

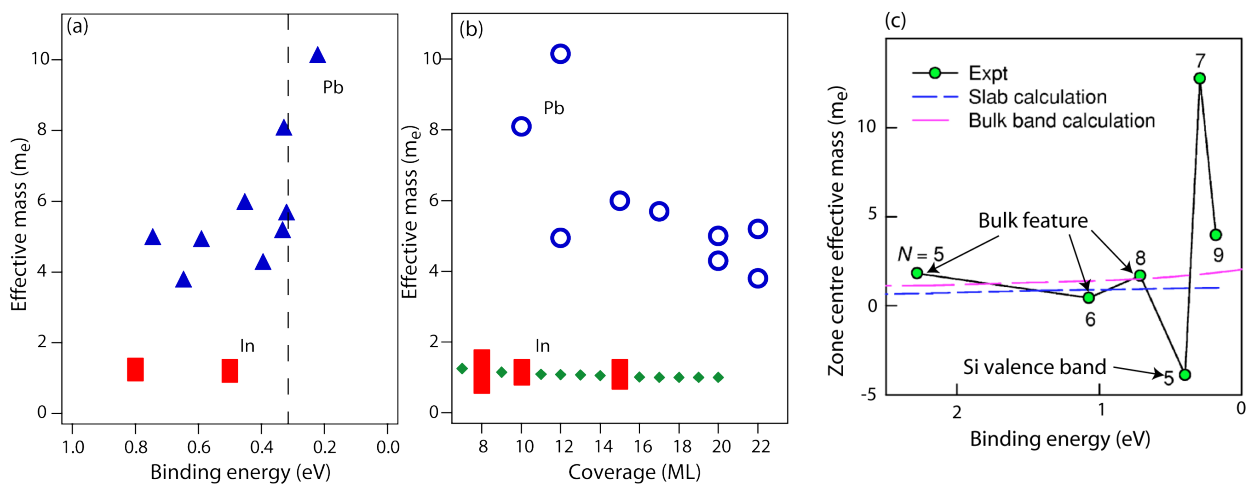


Figure 5.4: Effective mass of Pb (triangles and circles) and In (squares) quantum well states on Si(111) as a function of (a) binding energy and (b) coverage. The diamonds indicate the effective mass expected from theoretical considerations. The dashed line in (a) indicates the Si valence band maximum. (c) Effective mass as a function of coverage for Pb layers on Si(111) from Upton⁶; labels indicate data points which in my view cannot be ascribed to QWS.

The trend in effective mass as a function of binding energy is more complex. Starting from higher binding energy, there is first a plateau of relative constant m^* around $5 m_e$. At the Si valence band maximum (indicated by the dotted line), the effective mass increases, here it should be noted that these states belong to the lower coverages. In a recent paper by Upton *et al.*⁷ a much higher increase in m^* at the Si VBM is observed⁸ (here reproduced as Figure 5.4(c)). Upton *et al.* assume

7 M.H. Upton, T. Miller, and T.-C. Chiang, Phys. Rev. B **71**, 033403 (2005).

8 Due to a disagreement about the height of the wetting layer, the thicknesses mentioned in Ref. 7 are 1 ML higher than the numbering in this work. Ref. 7 also shows a disagreement with the layer thicknesses and QWS binding energies in a previous publication from the same authors¹⁰.

that the variations of the phase shift at the interface close to the Si band edge are responsible for the reported high effective masses; in other words, the band curvature is only mimicked by the interaction with the substrate. This argument seems to be supported by the observation that, far away from the Si VBM, the measured effective masses are close to theoretical expectations. Upton *et al.* also argue that the influence of the substrate band is so large that it can even result in a negative effective mass of the QWS in the overlayer material. Although this explanation seems tempting, it has some severe shortcomings, and because an identification of these shortcomings will also result in a better understanding of the problem, I will discuss some serious objections to this interpretation.

The data point for a 7 ML film in Figure 5.4(c) corresponds well with the data presented in Figure 5.4(a) and (b), although the higher effective mass leads to the suspicion that the hybridization with the substrate band was not incorporated in the fit. For this 7 ML thick film, the model based on a free-standing slab and the measurement show a similarly good match for the $6p_{x,y}$ derived states, and discrepancy for the $6p_z$ derived states, as shown in Figure 5.2. For the 5 ML thick layer from Upton *et al.*, the calculations and measurements show no correspondence for the highest occupied QWS. This can be explained by the fact that, at the indicated binding energy (~ 0.4 eV), there is actually no QWS; this feature arises from the Si valence band which can be observed due to the absence of an intense QWS. This directly explains the negative dispersion measured for this state, such that we can exclude this data point. Furthermore, the data for this coverage is obtained with a photon energy of 29 eV; at this excitation energy a direct transition is expected around 2.5 eV⁹. Combining this with the observation in Chapter 3 and 4 that for the system under investigation, no QWS have been observed at these high binding energies, which is also confirmed by Upton *et al.* in an earlier publication¹⁰, leads to the identification of this “QWS” as the bulk-like feature due to incoherent scattering. Because of its bulk background, this feature is expected to have an effective mass of approximately m_e . Along a similar line of reasoning, the states for 6 ML and 8 ML thick films can also be identified as the bulk-like feature, explaining their low effective mass. It is crucial that these states are outside the Si bandgap and no other QWS are observed for the same coverage, in contrast to predictions, and that the features occur exactly at the direct transition in ARPES. This interpretation is supported by the fact that, in the extensive data set for a wide coverage range presented in Figure 5.4(a) and (b) there is not a single QWS that has an effective mass less than 3.8 m_e . This means that only the 7 and 9 ML data points in Figure 5.4(c) remain. No data is shown for the 9 ML film, but the fact that this state is very close to E_F might have hindered the fitting process. Apart from this, the data for the 22 and 24 ML thick films in Figure 3.10 show that the curvature does not increase much for the QWS that are well above the Si VBM.

9 K. Horn et al. Phys. Rev. B **30**, 1711 (1984).

10 M.H. Upton et al. Phys. Rev. Lett. **93**, 026802 (2004).

From the above argument it is clear that the interpretation of the bulk-like feature as QWS is responsible for a misinterpretation of the ARPES data by Upton *et al.* The question then arises why this feature (not observed in the experiments for Pb on Si(111) $\sqrt{3}$ in the present work), may have such a profound influence. One of the reasons is that Upton *et al.* have deposited on the β phase of the Si(111) $\sqrt{3}$ reconstruction, whereas the experiments in this work have been performed on the α phase. The latter can be prepared defect free over larger distances, whereas the former can still result in a large number of buried scatterers¹¹. Another reason is that this bulk-like feature is always present, although with low intensity, and is normally overshadowed by the very intense QWS. When no QWS are present, as was the case for the 5, 6 and 8 ML thick islands in Figure 5.4(c), the contrast is enhanced in favour of low intensity features.

There are, however, other reasons why the explanation given by Upton *et al.* is likely to be inadequate. If we assume that the variations of the phase shift close to the band edge of the substrate bands influence the dispersion of the QWS in the overlayer material, this influence can be expected to depend on the distance from the band edge. When the state is further away from the substrate bands, the dispersion should increase, and vice versa. Due to the negative dispersion of the Si bands, the distance is smallest at the zone centre, and will increase with increasing k_{\parallel} . However, at $\bar{\Gamma}$ experiment and theory show an overlap in Figure 5.2, also in Ref. 7; the discrepancy increases with larger k_{\parallel} and therefore larger distance to the band edge. Furthermore, Wu *et al.*¹² have suggested that the influence of the substrate bands on the phase shift at the interface can be substantial for metallic substrates. The band dispersion in their metal substrate (cobalt) is, however, opposite to that in Si(111) here. Moreover, it is comparable to that of Cu, such that for Pb on Cu(111) an increase of effective mass should be expected, whereas for Pb on silicon the effect should be opposite, in contrast to the present observations.

The strongest argument against an explanation of the high effective mass on the basis of a k_{\parallel} dependent phase shift is provided by the comparison to indium and other simple metals on Si(111). The values of m^* for indium in Figure 5.4 are much lower than those of Pb, and the in-plane band structure in Figure 4.14 also shows a different behaviour. Away from the hybridization region around the zone centre, the In QWS follows the expected free-electron-like parabola, and experiences no influence of the substrate band structure. From this it can be concluded that the influence of the substrate band is limited to the region where these bands and the QWS actually cross. This means that the curvature of the QWS in Figure 5.3 outside this region directly represents the effective mass of the QWS, free from any influence of the substrate bands; this is supported by the strict parabolic behaviour in this region.

11 T.-L. Chan et al. Phys. Rev. B **68**, 045410 (2003).

12 Y.Z. Wu et al. Phys. Rev. B **66**, 245418 (2002).

For fully localized electrons, such as some molecular orbitals in adsorbed species or deeper lying core levels, the state is expected to show absolutely no dispersion in all \mathbf{k} directions. The measured QWS for Pb on Si(111) $\sqrt{3}$ closely resemble this behaviour, and are therefore expected to be highly localized in the in-plane direction. This localization strongly reduces the bandwidth W of the $6p_z$ derived bands: for most coverages W is below 50 meV. This bandwidth represents the kinetic energy of the electron, which, in order to determine whether electron correlation effects can play a role, should be compared to the electron interaction energy. When the kinetic energy is lower than the interaction energy, the electron cannot “escape” the influence of the other electrons. For Pb a definite value of the interaction energy has so far not been reported, but from a comparison to other BCS superconductors¹³ it can be estimated to be on the order of at least 0.1 eV. This means that the electrons in the $6p_z$ bands can experience strong electron-electron correlation effects. It is hard to predict what in this case the influence of electron-electron coupling on ARPES measurements is, but as described above, in photoemission this is likely to show up as a collection of satellite peaks caused by the additional excited states. Unfortunately it is not clear whether these features, if present, can be distinguished from the general background, as visible in Figure 3.9, for example.

The present interpretation of increased effective mass in terms of a thickness- and energy-dependent change in quantum well state dispersion caused by enhanced electron localization and, possibly, correlation, is supported by other experimental observations. First, the Hall effect in thin Pb films on Si(111) shows an oscillatory reversal of sign as a function of thickness^{14,15}, indicating a size quantization effect on the specific resistivity. This observation cannot be fully explained on the basis of electron confinement based either on free-electron like states, or on details of the Pb band structure in the (111) direction¹⁶. Electron correlation effects can have a profound influence on the Hall coefficient, hence a consideration of the large in-plane effective masses found here might be useful for an interpretation of the Hall effect observations. Second, Altfeder and co-workers have observed, in scanning tunnelling microscopy experiments, that the Si(111) 7×7 reconstruction can be imaged through Pb layers of more than 100 Å thickness¹⁷, suggesting that the lateral spread of electrons injected into the layer is extremely small. As discussed in Section 3.1.2, a similar effect in indium layers is restricted to very small thicknesses; in Figure 5.4(b) it can be observed that In layers at thicknesses of 8 ML and above have a low effective mass and no localization. Altfeder and co-workers have interpreted their STM results in terms of a large anisotropy of the effective masses associated with in-plane and transverse electron motion, in line with our interpretation above. The observation of atomic scale features in tunnelling experiments of electrons transmitted

13 W. Buckel, *Superconductivity; Fundamentals and Applications*, (VCH, Weinheim 1991).

14 M. Jalochoowski, M. Hoffmann, and E. Bauer, *Phys. Rev. Lett.* **76**, 4227 (1996).

15 O. Pfenningtorf, PhD thesis, Universität Hannover (2001).

16 I. Vilfan, M. Henzler, O. Pfenningtorf, and H. Pfnür, *Phys. Rev. B* **66**, 241306 (2002).

17 I.B. Altfeder, D.M. Chen, and K.A. Matveev, *Phys. Rev. Lett.* **80**, 4895 (1998).

through a Pb layer of considerable thickness on Si(111) shows that the “de-focusing” of the tunnelling electrons in an energy region close to the Fermi level is extremely small, demonstrating the lateral localization of such states. In a later publication¹⁸ the authors tried to explain the electron interaction by introducing a self-organized 2 dimensional Anderson lattice as the new ground state. In this picture the localized electrons are the impurities in the lattice, and a coulomb interaction results between the localized and delocalized electrons. Although this would explain some of the observations, it remains unclear why and how this new state is formed.

From the match between theory and experiment in Figure 5.2, it is clear that the bands derived from the $6p_{x,y}$ states remain unaffected; the localization seems to only occur in the $6p_z$ states. In an atomic orbital picture, this means that the overlap between the $6p_{x,y}$ orbits remains the same as in bulk Pb, whereas the in-plane overlap between the $6p_z$ states is reduced. X-ray diffraction (XRD) studies of the Pb/Si(111) system have revealed a bilayer oscillation in the interlayer spacing¹⁹, persisting also for higher coverages, that are not present in bulk Pb data. This indicates that the layer is not fully relaxed in the direction perpendicular to the substrate, and that the Pb atoms do not occupy their bulk equilibrium positions. We therefore suggest a structural rearrangement of the layer that minimizes the overlap of the $6p_z$ orbits in the direction parallel to the surface, but hardly affects the overlap of the $6p_{x,y}$ orbits. How this alteration occurs, and exactly what its results are, awaits a theoretical analysis. The origin of this structural rearrangement, however, directly follows from the ARPES data shown here. By increasing the localization in the $6p_z$ states, the bands that are derived from them will avoid a Fermi level crossing, or in other words, a gap will open up. This way, the system can significantly reduce its total energy, even when the temperature is too low to allow for the formation of preferred heights as observed for Pb/Cu(111) and Pb on graphite (see Section 3.2). For Pb/Si(111) $\sqrt{3}$ an energy balance between the energy reduction due to the avoided E_F crossing, and the energy gained due to the strain in the layer has to be considered. Considering that only very small displacements are necessary, the balance will most likely shift in favour of the structural alteration.

From ARPES data we thus find that the in-plane dispersion of the QWS in Pb on Si(111) is up to one order of magnitude larger than expected from calculations and in bulk states. From a comparison with In/Si(111), it is clear that this cannot be ascribed to the interaction with the substrate bands, as has been suggested by Upton *et al.* The determined high effective mass is an indication of electron localization in the direction parallel to the surface. From a comparison between the bandwidth of the QWS and the electron interaction energy, it follows that electron correlation effects may occur in these Pb films. The strong localization is most likely caused by a structural rearrangement to minimize the total energy of the layer, which results in a reduced overlap of the $6p_z$ states.

18 I.B. Altfeder, X. Liang, T. Yamada, D.M. Chen and V. Narayanamurti, Phys. Rev. Lett. **92**, 226404, (2004).

19 P. Czoschke, H. Hong, L. Basile, and T.-C. Chiang, Phys. Rev. Lett. **91**, 226801 (2003).

5.2 Electron-phonon coupling: In on Si(111)

The interaction between electrons and lattice vibrations, i.e. electron-phonon coupling (EPC), plays a decisive role in many phenomena in condensed matter physics, the most famous example being conventional superconductivity. It may also be the basis of high- T_c superconductivity^{20,21}, a phenomenon that is still not well understood. The two main parameters in EPC are the coupling strength λ and the phonon frequency ω_0 . Interaction between electrons and phonons is only expected to occur with these electrons within an energy window of $\hbar\omega_0$ around the Fermi level, which is, depending on the material, on the order of 100 meV. For a better understanding of the influence of electron-phonon coupling in ARPES, it is important to consider the photohole created by the photoemission process. For energies larger than $\hbar\omega_0$ away from E_F , this photohole can decay by emitting a phonon, because it has enough energy. When the energy is closer to the Fermi level, the photohole has insufficient energy to decay into phonons. In this energy range, the hole will continuously emit and reabsorb a phonon. As a result, the photohole will be “dressed with a cloud of virtual phonons”²², which in turn will lead to a higher effective mass compared to the non-interacting state. Thus, the band will have a different slope in the region within $\hbar\omega_0$ of the Fermi level, effectively leading to the formation of two branches of bands of the same state. This process is schematically sketched in Figure 5.5. In this process, the change in slope between the non-interacting and the interacting branch is determined by the mass enhancement factor $(1 + \lambda)$. This formation of separate branches has been observed in the surface state of W(110) upon the absorption of hydrogen and deuterium²². The renormalization factor between the separate bands in this experiment indicates a coupling to the stretch vibrational mode of the adsorbed species, λ obtained after the absorption of deuterium is therefore smaller than for the absorption of hydrogen because of its higher mass and hence lower vibrational frequency.

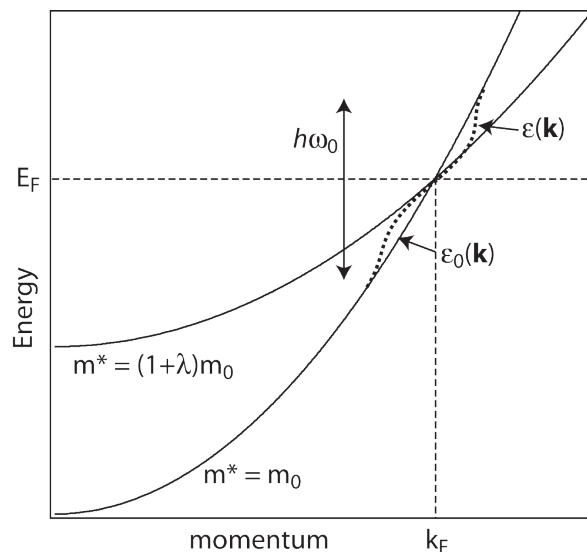


Figure 5.5: Illustration of the effect of electron-phonon coupling on the band structure in the vicinity of the Fermi edge. Note the formation of two separate band branches, one further away from E_F with effective mass m_0 , and one closer to E_F with effective mass $(1+\lambda)m_0$.

20 A. Damascelli, Z. Hussain, and Z.X. Shen, *Rev. of Mod. Phys.* **75**, 473 (2003).

21 A. Lanzara et al. *Nature* **412**, 510 (2001).

22 E. Rotenberg, J. Schaefer, S.D. Kevan, *Phys. Rev. Lett.* **84**, 2925 (2000).

As described before, interaction effects are characterised by the self-energy of the system under investigation. In photoemission, the real part of the self-energy represents the change in energy, of which the above discussion is an example, and which will be explained in more detail below. The imaginary part of the self-energy represents the change in line width due to many-body interactions. An accurate measurement of the line width of a state as a function of temperature can thus be used to extract λ and to obtain an indication of EPC strength. Such measurements have been performed in two systems related to the research in this work; for thin Ag films on Fe(100)²³ with well developed QWS, it was found that the electron-phonon coupling depends on the specific band the QWS are derived from. The d-derived states exhibit a λ which is a factor 35 smaller than for the sp-derived states, this difference is caused by the different hole relaxation paths. For Pb films on Si(111)7x7, λ was observed to oscillate as a function of layer thickness²⁴. The main advantage of this technique is that it does not rely on a band crossing E_F in order to observe EPC. However, a major disadvantage is that, by changing the temperature, the system under investigation may be adversely influenced. For many of the quantum well systems studied in the present work, a temperature change will destroy the layer, or will lead to the rearrangement into preferred heights with a different photoemission signature. This presents a serious shortcoming of this technique, such that its details will not be further discussed here.

The variation in band shape induced by electron-phonon coupling can be used to extract the full characteristics of this interaction, this has recently been shown by Shi *et al.*²⁵ for the S1 surface state of Be ($10\bar{1}0$). Because of the relevance of their approach to the results obtained in this work, it is summarized here.

All physical quantities related to electron-phonon coupling can be deduced from the Eliashberg function $\alpha^2 F(\omega; \epsilon, \hat{\mathbf{k}})$ ²⁶. This function describes the total transition probability of a quasiparticle from and to the state $(\epsilon, \hat{\mathbf{k}})$ by coupling to phonon modes with a frequency ω ²⁷. The real part of the self-energy, which is accessible to photoemission, can be expressed in terms of the Eliashberg function as

$$\text{Re}\Sigma(\epsilon, \hat{\mathbf{k}}; T) = \int_0^\infty \alpha^2 F(\omega; \epsilon, \hat{\mathbf{k}}) K\left(\frac{\epsilon}{kT}, \frac{\omega}{kT}\right) d\omega, \quad (5.8)$$

where $K(y, y') = \int_{-\infty}^\infty f(x-y)2y'dx/(x^2 - y'^2)$ and $f(x)$ is the Fermi distribution function. The real part of the self-energy can be calculated from the difference between the measured data and the quasiparticle dispersion without EPC. Especially for quantum well states and metal surface

23 J.J. Paggel, D.-A. Luh, T. Miller, and T.-C. Chiang, Phys. Rev. Lett. **92**, 186803 (2004).

24 Y.-F. Zhang et al. Phys. Rev. Lett. **95**, 96802 (2005).

25 J. Shi et al. Phys. Rev. Lett. **92**, 186401 (2004).

26 G. Grimvall, The Electron-Phonon Interaction in Metals, (North-Holland, Amsterdam, 1981).

27 A. Eiguren et al. Phys. Rev. Lett. **88**, 66805 (2002); A. Eiguren et al. Phys. Rev. Lett. **91**, 166803 (2003).

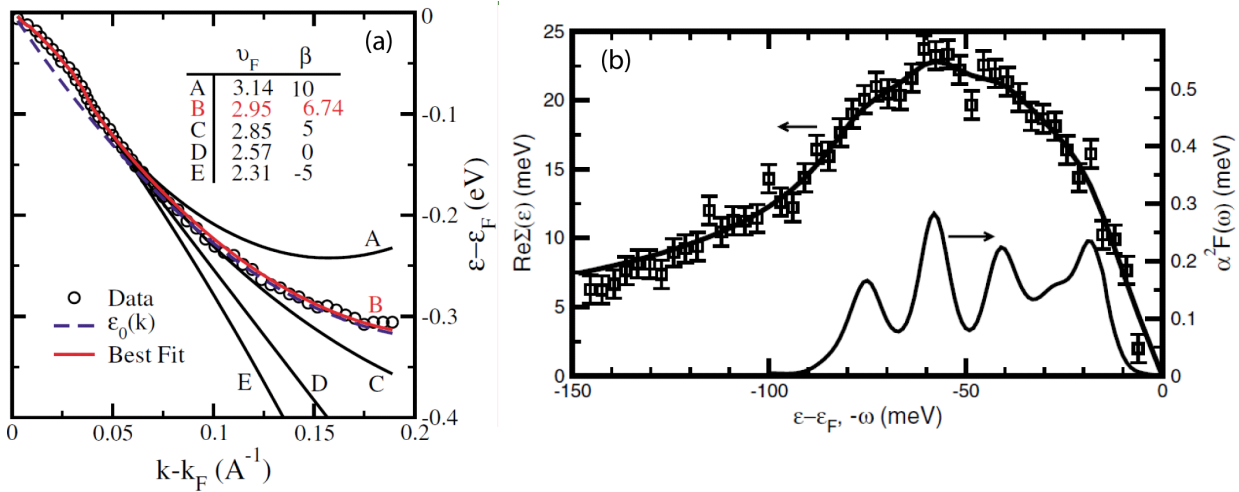


Figure 5.6: (a) Quasiparticle dispersion for the S1 surface state of Be ($10\bar{1}0$) (circles) with the possible parabolic fits indicated, the best fit is from the dashed line. (b) Real part of the self energy obtained from the difference between the measurement and parabolic fit in (a). The inset shows the extracted Eliashberg function. Figures from Shi²⁵.

states, the latter can be described by a parabola. In order to obtain an adequate fit for this parabola, enough data points outside of the energy range where EPC is expected to occur are needed. Figure 5.6(a) shows the measured dispersion of the Be ($10\bar{1}0$) surface state, together with several possible fits to obtain the non-interacting dispersion, from Shi *et al.* Taking the energy region further away from E_F into account, it is clear that line B provides the best fit. In a region of approximately 100 meV below the Fermi level, a deviation from the parabolic dispersion is visible. This deviation is comparable to the trend in Figure 5.5, and is interpreted as being due to electron-phonon coupling. Figure 5.6(b) shows the real part of the self-energy, obtained by direct subtraction of the data points and the non-interacting dispersion in Figure 5.6(a). The structure of this quantity $\text{Re}\Sigma(E)$ does not directly represent the phonon density of states, but gives a first indication of variations in the EPC strength.

The extraction of the Eliashberg function from the difference displayed in Figure 5.6(b), imposes an integral inversion problem. Due to the mathematical instability of the problem, it is not possible to simply use a least-squares method in the extraction process. This instability can be overcome by using the maximum entropy method²⁸ (MEM), with the additional advantage that physical constraints can be incorporated into the fitting process. These constraints for the Eliashberg function are that the function remains positive, and that it becomes zero at the Fermi level and for energies larger than a certain onset energy. The result of this approach for the data from Shi *et al.* is shown in as a inset in Figure 5.6(b). It can be seen that fluctuations in the real part of the self-energy are reflected in the Eliashberg function. A considerable advantage of the method described above is that it is rather insensitive to noise in the original data; the main features will remain the same. On the other hand, structural deviations in the data will destroy the integral inversion process. Once

the Eliashberg function is extracted, almost all properties of the electron-phonon coupling process can be derived from it. For example, the coupling strength and mass enhancement parameter λ can be extracted from the Eliashberg function as follows:

$$\lambda = 2 \int_0^{\infty} \frac{\alpha^2 F(\omega; \epsilon_F, \hat{\mathbf{k}})}{\omega} d\omega. \quad (5.9)$$

One advantage of determining λ directly from the Eliashberg function lies in the fact that no further assumptions need to be made regarding phonon models or measurement temperature.

Experiments based on the extraction of the real part of the self-energy from the photoemission data have been performed on the surface states of metals. Bulk derived bands cannot be used due to the final state broadening of these lines, which will overshadow the electron-phonon coupling process. However, using a surface state to derive EPC parameters will only yield information about the *characteristics of the surface of the crystal*, which may differ substantially from the bulk properties. This problem can be overcome by using quantum well states for the determination of EPC parameters. As described several times throughout this work, QWS are directly derived from the bulk band of the metal in which they are formed. Furthermore, the electron propagation is not confined to the surface regions of the layer. Due to the fact that QWS are, just as surface states, confined in the k_z direction, final state induced broadening will be absent, and the line width directly represents the intrinsic line width of the state. Moreover, due to the lack of confinement in the direction parallel to the surface, QWS can generally be well described by a free-electron-like parabola, which makes the process of determining the non-interacting band relatively easy. The combination of these effects renders QWS ideally suited for the direct measurement of electron-phonon coupling in bulk metals. However, up to this moment no experiments of this kind have been performed. Given our experience with QWS, we have attempted use them for λ derivation. However, this is a test experiment; compared to the data reported in the rest of this thesis a lower temperature and better spectral resolution is necessary. Still, here we will show that a direct measurement of the real part of the self-energy is possible for QWS formed in layers of In on Si(111).

Figure 5.7(a) shows a cut through the SBZ along the $\bar{\Gamma} - \bar{K}$ direction for a 17 ML thick film of In on Si(111). This relatively thick film has been chosen to minimize the influence of the interface and possible strain on the electron-phonon coupling process. Comparable to data shown in Section 4.4, a strong hybridization between the In QWS and the Si substrate can be observed. This interaction is, however, limited to the region around the zone centre. Because of the absence of Si bands in the energy and momentum region where the upper QWS crosses the Fermi level, it is safe to assume that any deviations in the dispersion of the band are not due to interaction with the substrate bands. The region that we will focus on, is marked by the circle. This area has been measured again with

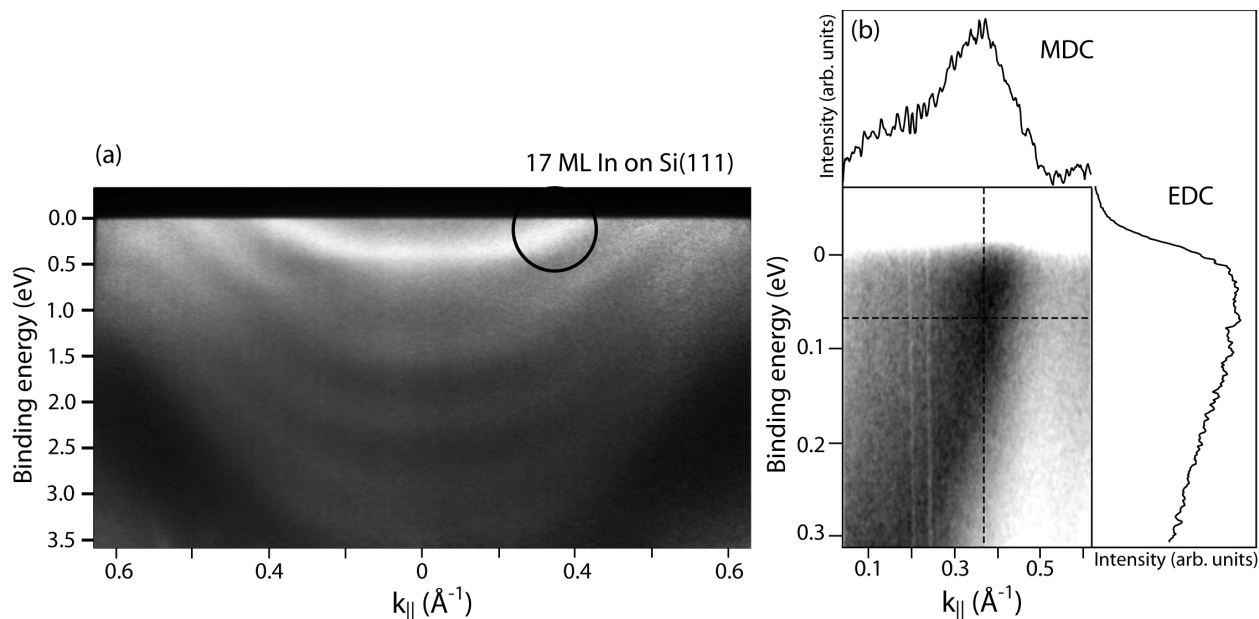


Figure 5.7: (a) Cut through the SBZ along $\Gamma - K$ for a 17 ML thick In layer on Si(111) acquired with a pass energy of 20 eV at a photon energy of 26 eV. The circle indicated the part of the image that is magnified in (b) with pass energy 5 eV. Note that in (b) the colour code is inverted. The dashed lines in (b) indicate along which line the EDC and MDC have been extracted shown on the side and top.

the same slit settings and a pass energy of 5 eV, in order to increase the energy resolution even further. At the settings used in this experiment, the energy resolution from the monochromator is less than 5 meV; the total energy resolution is determined from the width of the Fermi edge to be 45 meV (EDC in Figure 5.7(b)) and the angular resolution is, as described in Chapter 2, better than 0.25° . The close-up image obtained with this resolution is shown in Figure 5.7(b). In this image, intensity seems to extend beyond the Fermi edge. This is due to two reasons: first, the energy scale is rather small, and second the contrast of the image has been enhanced in order to clearly see the QWS band. In the region between the Fermi energy and a binding energy of 100 meV, a deviation from the parabolic dispersion of the QWS is visible. The intensity seems to shift towards lower k_{\parallel} values, comparable to the EPC sketch in Figure 5.5 and the measured data in Figure 5.6(a). Considering this similarity and the energy range of less than 100 meV, this deviation from the free electron like parabola is likely to be caused by electron-phonon coupling.

In order to derive more quantitative statements, it is necessary to first perform a fit of the data to extract the peak binding energy position as a function of in-plane momentum. In the previous section, energy distribution curves (EDC) were extracted from the image, and these were fitted with a Fermi function and a Voigt peak, which resulted in exact peak positions. On the right-hand side of Figure 5.7(b) an EDC is shown, extracted from the image along the vertical dashed line. The absence of any clear features apart from the Fermi edge in this spectrum indicates that, for this data set, a different approach is necessary. The top of Figure 5.7(b) shows a spectrum

obtained along the dashed line of constant energy. This so-called momentum distribution curve²⁹ (MDC) shows a clear peak that rises well above the noise level. The possibility to either extract an EDC or MDC from the data shows another advantage of image-type electron energy analysers. Unfortunately, a clear description of the background of an MDC, unlike for a typical EDC, does not exist. Therefore, the background was fitted with a third order polynomial based on the data points further away from the peak. The peak itself was fitted with a Lorentzian line shape, because in previous measurements³⁰ this has proven to give the best results for the fitting of features in an MDC.

The peak positions obtained from this fitting procedure are shown in Figure 5.8(a), along with the parabola representing the non-interacting quasiparticle, marked with $\epsilon_0(\mathbf{k})$. The effective mass that can be determined from the curvature of this parabola is equal to $1.1 m_e$, which is consistent with the results for In shown in the previous section. The deviation of the data in the binding energy range below 80 meV from the non-interacting dispersion curve is reproduced in the fit, and shows a strong similarity to the data in Figure 5.6(a). The real part of the self-energy can now be obtained by subtracting the binding energy of the parabolic fit from the peak positions obtained from the data. The resulting difference is shown in Figure 5.8(b) as a function of quasiparticle binding energy. In the region between 70 meV and the Fermi level, the real part of the self-energy deviates from zero with around 20 meV, a value that is comparable to the magnitude in Figure 5.6(b). This indicates that this deviation is due to the influence of electron-phonon coupling. At the Fermi level

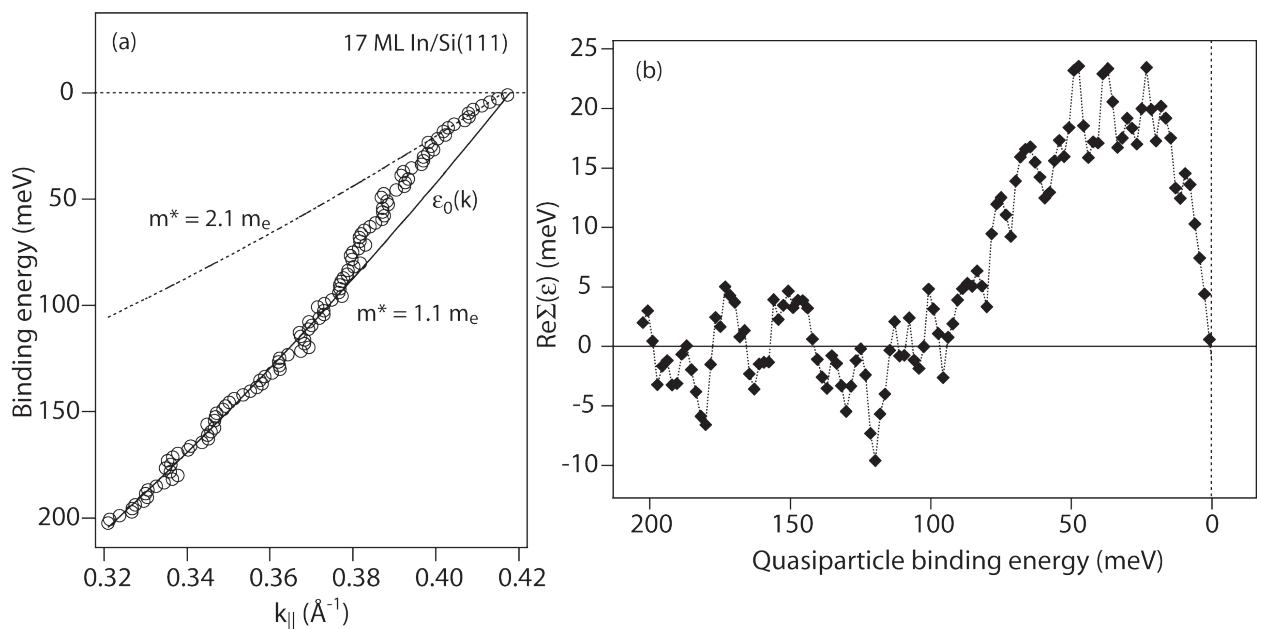


Figure 5.8: (a) Quasiparticle dispersion obtained by fitting the MDCs from Figure 5.7(b) as described in the text. The solid line indicated by $\epsilon_0(\mathbf{k})$ represents a parabolic fit to the data point at higher binding energy, the dashed line is a parabolic fit to the data points close to E_F . (b) Real part of the self energy extracted from the difference between the data points and $\epsilon_0(\mathbf{k})$ as a function of quasiparticle binding energy.

29 T. Valla et al. *Science* **285**, 2110 (1999).

30 S. LaShell, E. Jensen, and T. Balasubramanian, *Phys. Rev. B* **61**, 2371 (2000).

the influence of EPC diminishes (see Figure 5.5) and the real part of the self-energy approaches zero again. The magnitude of the deviation of $\text{Re}\Sigma$ from zero between 80 meV and the Fermi level is much larger than the noise level in the part of the data that is not affected by electron-phonon coupling. Fluctuations in this deviation are, however, of the same magnitude as the noise. A direct extraction of the Eliashberg function seems therefore not viable, especially because the noise has a systematic origin. This can be verified from the raw data shown in Figure 5.7(b); at approximately 2 and 2.5 \AA^{-1} , two vertical lines can be recognised. In the data there are more of these lines, albeit less intense, as can be induced from the structured “noise” in the MDC. The origin of these stripes lies in imperfections on the entrance slit of the analyzer. The electric field is locally distorted due to these defects, resulting in a lower throughput of electrons. This phenomena arises within a certain combination of slit size, pass energy and kinetic energy, and is typical for most image-type analyzers. In the present situation, a larger slit size or higher pass energy (see Figure 5.7(a)) would have solved the problem, but with those settings the energy resolution necessary for electron-phonon coupling measurements is unattainable. Although a complete analysis of all electron-phonon coupling parameters is thus not possible, the data in Figure 5.8 show that information about the *coupling strength in bulk metals* is certainly obtainable by high resolution band structure measurements of quantum well states.

As indicated in Figure 5.5, the mass enhancement parameter λ can directly be deduced from the deviation from the parabolic behaviour in Figure 5.8(a). A second parabola is added that intersects with the non-interacting quasiparticle dispersion at the Fermi level. This parabola represents the mass enhancement of the band due to the interaction with phonons, and has an effective mass of $(1+\lambda)$ times the effective mass obtained for the non-interacting branch. A value of 0.9 for λ provides the best fit of the upper part of the band, which is consistent with recent *ab initio* calculations for bulk In^{31} .

The experiments presented in this section have opened the door to the determination of electron-phonon coupling in bulk metals through angle resolved photoemission spectroscopy on quantum well states. However, there are some technical considerations; the difference between the shape of the measured curve and the structure predicted for the non-interacting behaviour due to EPC is determined to be around 20 meV. Furthermore, in order to extract the Eliashberg function, variations of less than 10 meV should be measured within a noise level of approximately 1 meV. This sets extreme standards for the measurements; the energy and angular resolutions should at least be below 50 meV and 0.25° respectively. This demand has been fulfilled in the experiments shown here, hence the deviation from the non-interacting band could be determined. The second demand is that the noise in the data should be as low as possible, and that systematic deviations in the data have to be absent. Ideally one would therefore perform the measurements on systems that in photoemission exhibit very intense and sharp peaks due to the QWS. From the data in this thesis, one might conclude that thin Pb overlayers form a perfect candidate for the extraction of

31 S.P. Rudin, R. Bauer, A.Y. Liu, and J.K. Freericks, Phys. Rev. B **58**, 14511 (1998).

EPC parameters for the bulk material. However, due to the tendency of Pb layers to rearrange their structure in order to reduce the total energy of the layer, no well-developed QWS have been observed in Pb that cross the Fermi level. At sufficiently low temperatures, the self-organization of Pb on graphite into islands of preferred height is likely to be suppressed, such that layer thicknesses form for which a QWS crosses the Fermi level. An additional advantage is that these reduced temperatures increase the spectral resolution of the experiment, and therefore enhance the quality of the data. Because of the low atomic mass, Be has a broad phonon spectrum. Furthermore, for surface states of this metal the Eliashberg functions has already been extracted³², which makes Be another good candidate for the measurement of the Eliashberg function in the bulk metal. Parallel to the work presented in this thesis, experiments on Be on Si(111) have been performed. However, due to the large intermixing of both materials, smooth layers that could accommodate QWS were not formed. An alternative substrate for the growth of smooth Be layers may be the graphite surface also used in other experiments in this thesis, or a W surface, because of the low reactivity of both materials.

Through the correct combination of substrate, interface reconstruction, deposition temperature, and post-deposition treatment of the layer, for those s-p-metals that show quantum well states, the possibility of a direct measurement of electron-phonon coupling parameters through angle-resolved photoemission spectroscopy opens up. The self-organization and interface-related phenomena discussed in this thesis may be of assistance in the choice of the right system and preparation conditions for these experiments.

In conclusion, the photoemission results presented here demonstrate the observation of electron-phonon coupling in QWS formed in In/Si(111). From the measurements, the real part of the self-energy can be determined, which differs from zero, in a manner expected from previous surface state experiments²⁵, in the energy region between E_F and 80 meV. Due to the influence of systematic errors in the data, the extraction of the Eliashberg function is difficult, but the bulk electron-phonon coupling parameter can be deduced from the deviation of the quasiparticle dispersion from the non-interacting free-electron-like parabola, and is found to be consistent with recent *ab initio* calculations for bulk indium.

